NUMERICAL INVESTIGATION ON PULSE DETONATION ENGINE PERFORMANCE UNDER DIFFERENT EQUIVALENCE RATIO

UDC:621.43.019.4:519.6
Original scientific paper https://doi.org/10.46793/adeletters.2024.3.1.1

Osman Kocaaslan[1]

[1]Selçuk University, Huğlu Vocational School, Department of Machinery and Metal Technologies, Konya City, Türkiye

Abstract:
Detonation-based engines have a higher thermal efficiency than deflagration-based engines and are therefore widely studied. In this study, the effect of initiation conditions on the detonation wave propagation and the performance of a pulse detonation engine, one type of detonation-based engine, was numerically investigated. Hydrogen-oxygen mixtures with equivalence ratios of ϕ=0.8, 1.0, and 1.2 were defined as initiation conditions with constant pressure and temperature. The numerical simulations were conducted using the transient explicit density-based solver in the ANSYS Fluent commercial software. The adaptability of the adaptive mesh refinement method in detonation-based engines was explored in the numerical studies, reducing the average total cell count by a factor of 2.617, and obtaining consistent results according to validation studies. The adaptive mesh refinement method was also used in numerical simulations where different equivalence ratios were defined. It was determined that an increase in the equivalence ratio resulted in an increase in the detonation wave velocity. Also, an increase in thrust distribution at the nozzle exit was observed before the blowdown stage, and the calculated thrust values for ϕ=0.8, ϕ=1.0, and ϕ=1.2 were 248.28 N, 264.5 N, and 270.83 N, respectively.

ARTICLE HISTORY
Received: 11 January 2024
Revised: 9 March 2024
Accepted: 22 March 2024
Published: 31 March 2024

KEYWORDS
Detonation wave, combustion, pulse detonation engine, computational fluid dynamics, adaptive mesh refinement, equivalence ratio

1. INTRODUCTION

In detonation waves, which are considered as the combination of shock wave and chemical reaction front, the shock front compresses the fresh fuel-oxidizer mixture. It causes an increase in temperature and pressure in this region [1,2]. The energy release produced in the detonation wave front by chemical reactions supports the propagation of the detonation wave. In detonation applications, lower entropy production is achieved compared to deflagration, and therefore, it has higher thermodynamic efficiency than deflagration [1,3]. When the detonation combustor is integrated into an engine cycle, the increment of thermal efficiency is nearly 20% greater than the deflagration combustor, and the reduction of fuel consumption is approximately 9% [4-5]. Bigler et al. [6] used Brayton and Humprey cycles to compare detonation and deflagration cycles. The Humprey cycle adds heat with constant volume instead of heat adding with a constant pressure process. At the same initial pressure, thermal efficiency increases by 9.8% in the ideal Humprey cycle according to the ideal Brayton cycle. Sousa et al. [7] examined thermodynamic and non-isentropic processes to compare deflagration and detonation using TRI60-5 turbojet engine experimental results. At the lowest compression ratio, the efficiency of detonation is 8% higher than deflagration. Suzuki et al. [8] stated that detonation-based engines are 13% more efficient than conventional thermal engines.

CONTACT: Osman Kocaaslan, e-mail: okocaaslan@selcuk.edu.tr

Pulse detonation engines, one of the detonation-based engines, have five stages in a cycle: filling, ignition, deflagration to detonation (DDT), expansion, and purge [9]. In the filling process, the detonation tube is filled with the fresh fuel-oxidizer mixture. After the ignition process, the flame is converted into a detonation wave using detonation to deflagration mechanisms such as Shchelkin spiral and obstacles. Expansion waves are produced when the detonation wave leaves from the detonation tube. In order to ensure a new cycle in the pulse detonation engine, the detonation tube must be cooled, and the products must be discharged from the detonation tube (purge step). In the purge step, a species that will not cause a reaction is transferred to the detonation tube, and the pulse detonation engine is ready for the next cycle [10,11].

With significant advancements in computational capabilities, various complex flow structures in aviation applications, such as shock front and flow separation development at different angles of attack for airfoils, deflagration applications, etc., can be validated through CFD analyses [12,13]. In literature, many studies include ignition and DDT processes for the propagation of the detonation wave in the pulse detonation engines. Obstacle [14-22] and Shchelkin sphiral [23-27] are used as DDT mechanisms. In numerical studies on the flame's transition into a detonation wave, the filling stage is not included, and the fuel-oxidizer mixture is defined as premixed in the detonation tube. Alam et al. [14] investigated the effects of different equivalence ratios on the DDT transition step and the detonation wave propagation using a pulse detonation engine configuration modeled with obstacles having a 0.5 blockage ratio. Tangirala et al. [17] utilized ideal and benchmark tube pulse detonation engine configurations in their numerical studies, examining the DDT and blowdown stages in experimental work. It was noted that consistent results were obtained in experimental studies for pulse detonation engine configurations using benchmark tubes. Debnath and Pandey [23] numerically examined the DDT phase and flame propagation in single-tube pulse detonation engine models, incorporating the Shchelkin spiral. The numerical studies concluded that the detonation wave strength was stronger in the pulse detonation engine model with the Shchelkin spiral.

Pulse detonation engines operating frequencies are in the range of 100-200 Hz. Filling and purge stages in the pulse detonation engines are time-consuming, and the effect of these stages on the operating frequency of the pulse detonation engine is critical [28]. Considering the operating frequency of the pulse detonation engine, it is necessary to achieve the prescribed equivalence ratio for the fuel-oxidizer mixture during the filling process in the detonation tube. The mixture efficiency obtained prior to initiating the detonation wave and the equivalence ratios of the fuel-oxidizer mixture directly influence the propagation of the detonation wave and the resulting thrust distribution. In this study, the effects of initiation conditions on detonation wave propagation and pulse detonation engine performance were numerically examined. Filling and purge steps were disregarded in the numerical simulations. A pulse detonation engine model, including a detonation tube and nozzle, was used in the validation study. Following the validation study, an outlet domain behind the nozzle was created to investigate the DDT and blowdown stages. As the initiation condition, the detonation tube was filled with a premixed fuel-oxidizer mixture at different equivalence ratios (ϕ = 0.8, 1.0, 1.2). The numerical study results were used to analyze the detonation wave propagation and variables, DDT and blowdown stages, and pulse detonation engine performance.

2. MATERIALS AND METHOD

2.1 Physical Model and Mesh Details

The pulse detonation engine configuration used in the reference study includes a detonation tube and a nozzle. In the numerical simulations, the pulse detonation engine configuration was modeled in 2D, and the geometric details are presented in Fig. 1. The detonation tube diameter (D_{PDE}) and length (L_{PDE}) for the pulse detonation engine configuration are 3.8 mm and 100 mm, respectively. The nozzle has a conical half-angle of 10°, and the expansion area ratio is approximately 8.1 [29].

Two numerical domains were created for numerical studies. The pulse detonation engine configuration containing the detonation tube and nozzle, as shown in Fig. 1 (a), was used for the validation study. As the second pulse detonation engine configuration, an outlet domain was added behind the nozzle, as seen in Fig. 1(b), to examine the DDT and blowdown stages. The outlet domain was extended upstream to support detonation wave propagation during the blowdown stage [29].

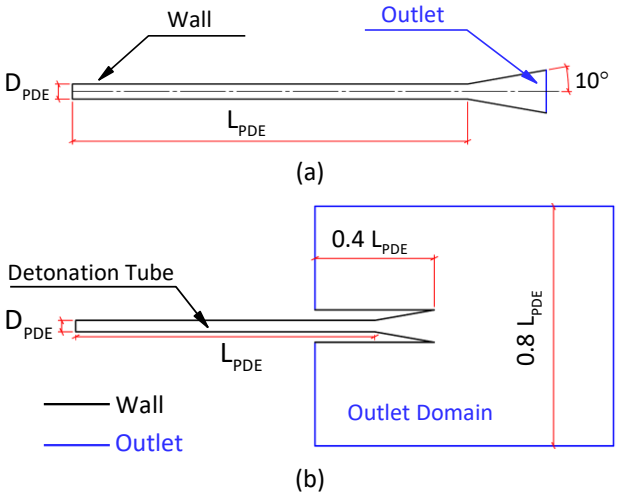

Fig. 1. Numerical domains used for a) validation and b) different initial condition cases [29]

The mesh structure used for validation studies employed constant cell sizes ranging from 0.1 to 0.37 mm. The total cell numbers for the detonation tube and nozzle are 21.750 and 2.871, respectively. The mesh structure's maximum and average aspect ratio values

In the numerical investigations carried out to analyze initial conditions, the adaptive mesh refinement (AMR) method was utilized. This approach, illustrated in Fig. 2, involves two main phases: cell refinement and coarsening. The primary cell is split into four equal-area cells in each refinement stage, effectively halving the cell sizes in the refined mesh region. Conversely, the coarsening process reverses this by merging previously divided cells and doubling the cell size with each stage. A variable and its limits were established to control the refinement and coarsening processes in the AMR method. Pressure gradient values increased cell count in regions like the detonation wave and wave fronts. The AMR method was executed in three stages, ensuring that cell sizes remained below 0.1 mm throughout the flow domain.

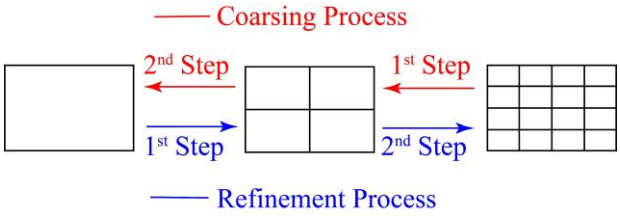

Fig. 2. Adaptive mesh refinement method

2.2 Numerical Method

Numerical studies were conducted using the ANSYS Fluent commercial software. Zhang et al. [1] numerically examined the effects of viscosity, mass diffusion, and thermal conduction on the propagation of detonation wave variables in rotating detonation engines. They indicated that the boundary layer has a negligible effect on the detonation wave velocity and that the pressure in the boundary layer is nearly constant. Therefore, in numerical studies focused on detonation-based engines, viscosity, mass diffusion, and thermal conduction can be neglected, and the two-dimensional governing equations are reactive Euler equations [30-35]. The Euler equations with source terms in Cartesian coordinates are expressed in Equation (1) [36].

$$\frac{\partial \vec{Q}}{\partial t}+\frac{\partial \vec{F}}{\partial x}+\frac{\partial \vec{G}}{\partial y}=\vec{S} \tag{1}$$

$$Q=\begin{bmatrix}\rho\\ \rho u\\ \rho v\\ \rho E\\ \rho Y\end{bmatrix}, F=\begin{bmatrix}\rho u\\ \rho u^2+p\\ \rho uv\\ \rho uH\\ \rho uY\end{bmatrix}, G=\begin{bmatrix}\rho v\\ \rho uv\\ \rho v^2+p\\ \rho vH\\ \rho vY\end{bmatrix}, S=\begin{bmatrix}0\\0\\0\\0\\ \dot{\omega}\end{bmatrix} \tag{2}$$

In the Eqn. 2, Q represents conservative variables, F and G are convective fluxes, and S is the source term. Y, $\dot{\omega}$, u, v, and w represent the mass fraction, mass production rate, and velocity components of reactants, respectively. The ideal gas approach is adopted for all species. The mixture density and pressure are determined by the relationships given in Equation (3) and Equation (5). The total energy equation is provided in Equation (6) [37]. In the equation given in Equation (6), e represents internal energy, and U is velocity [38].

$$\rho=\sum_{k=1}^{N_s}\rho_k \tag{3}$$

$$\rho_k=\rho Y_k \tag{4}$$

$$p=\sum_{k=1}^{N_s}\rho_k\frac{\bar{R}}{Mw_k} \tag{5}$$

$$E=e+\frac{U^2}{2} \tag{6}$$

In numerical analyses, a transient density-based solver was utilized. The Advection Upstream Splitting Method (AUSM) was employed for convective fluxes [38]. The least-squares-cell-based method was used for solving gradients. The reaction

rate constants were obtained through the Arrhenius equation. In Equation (7), where k_f represents the reaction rate, E_a is the activation energy, R is the gas constant, and T is the temperature, the Arrhenius equation is provided [39]. A 19-step irreversible chemical reaction mechanism was used to determine the reaction rates [40].

$$k_f = AT^b \exp\left(-E_a/RT\right) \quad (7)$$

To initiate the detonation wave, the detonation tube is filled with a premixed fuel-oxidizer mixture. The pressure and temperature values of the fuel-oxidizer mixture are 1 atm and 298 K, respectively [29]. A small flow field with high pressure and temperature (35 atm and 3000 K) is patched for the ignition process. The outlet domain is filled with air; the pressure and temperature values are 1 atm and 298 K, respectively. A pressure-outlet boundary condition is defined for the outlet boundary, set at 1 atm. The walls of the detonation tube are considered non-slip and adiabatic.

3. RESULTS AND DISCUSSION

3.1 Model Validation

In the reference experimental studies, pressure measurements were conducted at five different points along the detonation tube (L/L_{PDE}=0.299, L/L_{PDE}=0.450, L/L_{PDE}=0.602, L/L_{PDE}=0.754, and L/L_{PDE}=0.976) to examine pressure profiles and the propagation of the detonation wave [29]. Detonation wave velocity was obtained with the flame position along the detonation tube. Experimental studies indicated a detonation wave velocity of 2737 m/s. This value is approximately 96.51% of the Chapman-Jouguet (C-J) velocity [29].

The pressure profiles at specified points along the detonation tube in the reference experimental study are provided in Fig. 3. When examining the pressure profiles, it is observed that a sudden increase in pressure occurs at the detonation wave front, followed by a rapid pressure drop. Analyzing the pressure profiles in the reference experimental study, it is noted that the pressure profile at the point L/L_{PDE}=0.299 is associated with the DDT stage. At this point, the pressure value at the detonation wave front is approximately 9 atm. This value represents about 0.479% of the C-J pressure (p_{CJ}=18.779 atm). The nearly identical pressure peaks after the position L/L_{PDE}=0.45 indicate the termination of the DDT stage at this point [29].

When examining the pressure profiles obtained in the validation study, it is observed that trends similar to those in the reference experimental study are obtained. In the reference experimental study, notable differences in pressure peaks at L/L_{PDE}=0.299 and L/L_{PDE}=0.45 points are related to the DDT step. Beyond the L/L_{PDE}=0.45 point, the pressure peaks appear to stabilize and become nearly identical. In the numerical validation results, the pressure peaks at L/L_{PDE}=0.299 and L/L_{PDE}=0.45 points are recorded as 17.02 atm and 17.58 atm, respectively. These findings suggest that the DDT phase occurs more rapidly in numerical simulations. Furthermore, past the L/LPDE=0.45 position, the pressure development profiles exhibit consistent distributions, with the average pressure value at the detonation wave front determined to be 17.55 atm.

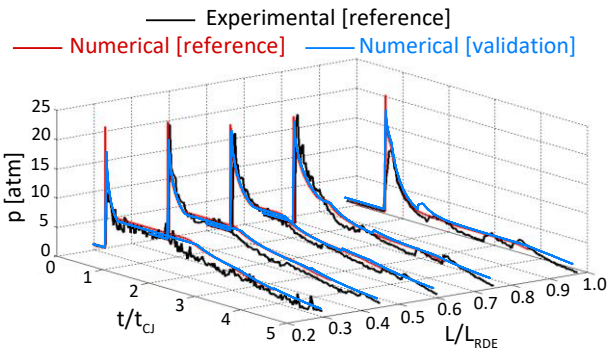

Fig. 3. Time evolution of pressure along the detonation tube [29]

In the validation study, the detonation wave was initiated using the direct ignition method. The t_{CJ} value was calculated taking into account the propagation of the detonation wave within the detonation tube and nozzle and it is 42.27 µs. When examining the propagation of the detonation wave given in Fig. 4, it is observed that the DDT stage is completed approximately after t/t_{CJ}=0.01.

In Fig. 4, it is determined that the detonation wave velocity is nearly constant. The detonation wave velocity measured in the reference experimental study is 2737 m/s [29]. The detonation wave velocity obtained from numerical studies is 2614 m/s; this value is 95.55% and 92.17% of the reference experimental study and the C-J velocity, respectively.

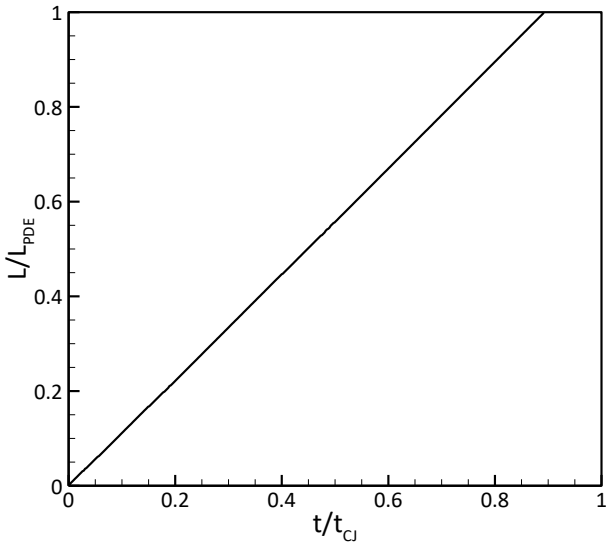

Fig. 4. Flame position along the detonation tube

3.2 Performance of Adaptive Mesh Refinement Method

The numerical solutions were conducted using two different mesh structures. The short durations required for the formation and decomposition of species in chemical reactions and the complex flow structure increase the requirements in numerical studies. Lietz et al. [41] utilized a mesh structure consisting of 140 million cells for their Large Eddy Simulation (LES) studies on the rotating detonation rocket engine. Sato and Raman [42] conducted numerical studies on an ethylene/air-based rotating detonation engine using a mesh structure with 30 million cells. To address the mentioned high demands, the adaptive mesh refinement method was employed in numerical studies. In this method, the pressure gradient variable was defined for the division and recombination of the cells.

The performance of the AMR method was examined in two steps. Firstly, the AMR method was applied using the validation domain in Fig. 1(a) and compared with the numerical validation results using constant cell size. In the second step, the domain given in Fig. 1(b) was used, and mesh development during the blowdown stage was investigated. When examining the cell development shown in Fig. 5, it is observed that the cell density is increased behind the detonation wave. The cells were recombined to form the primary cells in the regions where the pressure gradient distribution is outside the defined limits.

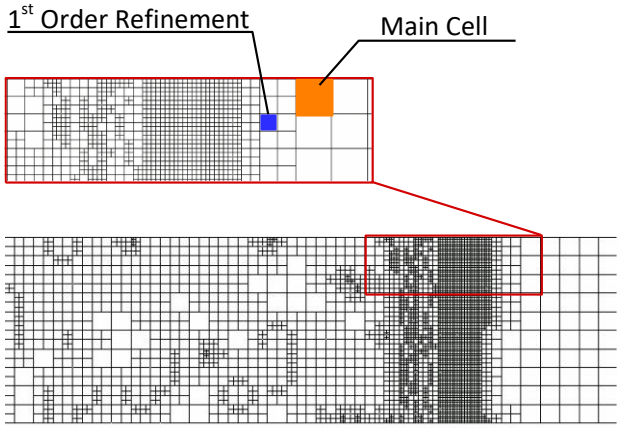

Fig. 5. Mesh structure in the detonation tube at t=30 µs

When examining the pressure development along the detonation tube given in Fig. 6, similar trends were identified in numerical studies using the AMR method and constant cell size. In the validation study where the AMR method is employed, higher pressure values are obtained at the detonation wave front compared to the validation study using constant cell size. The steady detonation wave front pressure in the validation studies using constant cell size and the AMR method is 17.55 atm and 18.5 atm, respectively.

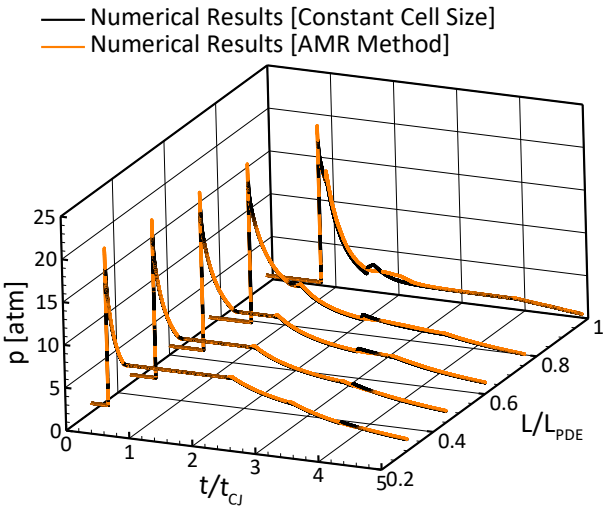

Fig. 6. Pressure distribution along the detonation tube

The reduction in the number of mesh cells decreases the computational requirements, but appropriate cell sizes need to be established for the stable propagation of the detonation wave. With the AMR method, the total number of cells is reduced, and cells of approximately 0.1 mm are created at the detonation wave front. Fig. 7 provides the development of the flame position and the cell number ratios (n_C) for examining the gains of the AMR method. The cell number ratio is obtained with the relationship given in Equation (8).

In the Equation (8), n_{AMR} and $n_{CONS.}$ variables are, respectively, the total number of mesh cells with the AMR method and the total number of mesh cells with constant cell sizes.

$$n_C = \frac{n_{AMR}}{n_{CONS.}} \quad (8)$$

When examining the detonation wave propagation given in Fig. 7, it is determined that, in the AMR method and the constant cell size numerical validation studies, the DDT stage is completed at t/t_{CJ}=0.118 and t/t_{CJ}=0.01, respectively. Subsequently, stable detonation wave propagation occurs. It is observed that the mesh ratio increases to 0.526 at t/t_{CJ}=0.165. This situation is related to regimes where the rapid pressure change behind the detonation wave is observed and the high-pressure region in the direct ignition zone. During the propagation of the detonation wave in the detonation tube, the average cell number ratio with the AMR method is determined to be 0.382.

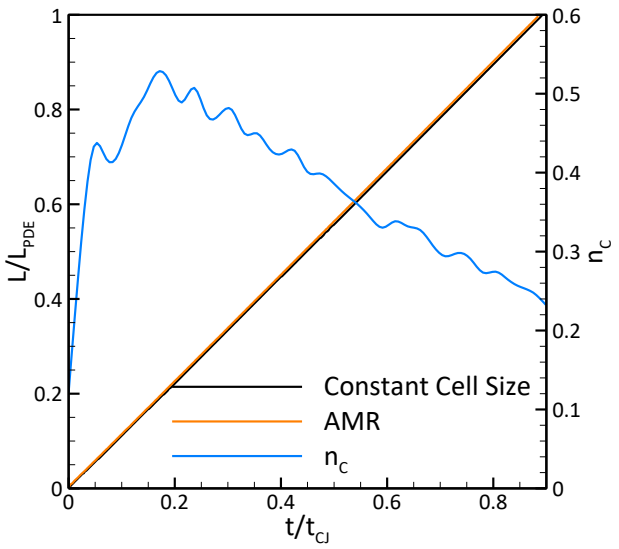

Fig. 7. Flame position and time evolution of the mesh cell ratio

Pressure gradient limits for the AMR method were defined at values suitable for examining the characteristics of detonation wave propagation during the blowdown stage. As seen in Fig. 8, the increase in cell density is maintained at the nozzle and during the blowdown stage at the detonation wave front.

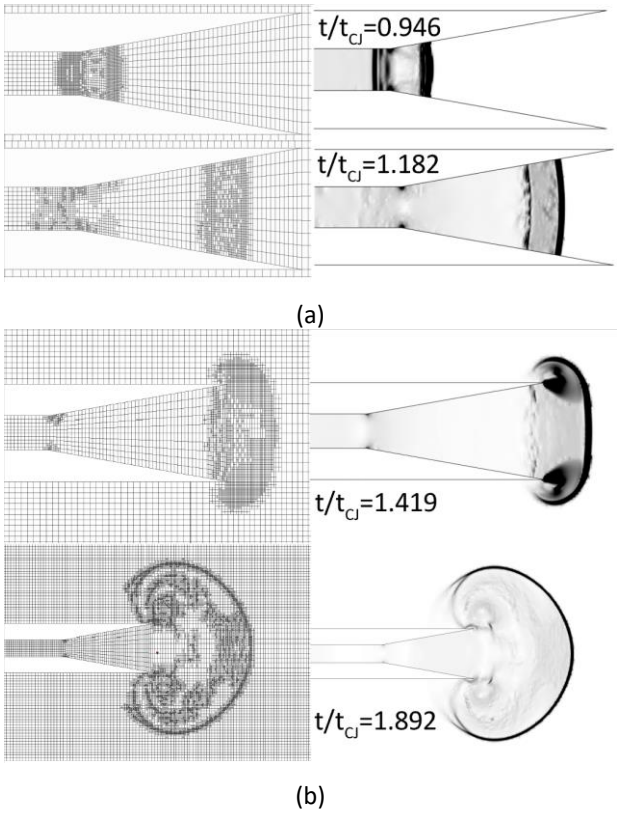

Fig. 8. Detonation wave propagation and mesh evolution a) in the nozzle and b) outlet domain

3.3 Detonation Wave Propagation and Nozzle Performance

Detonation wave propagation and changes in pulse detonation engine performance were investigated by filling the detonation tube with a fuel-oxidizer mixture with different equivalence ratios for rich, stoichiometric, and lean combustion. The equivalence ratios for rich and lean combustion are 1.2 and 0.8, respectively. The pressure and temperature of the fuel-oxidizer mixture filled into the detonation tube before ignition were kept constant, with values of 1 atm and 298 K.

In Fig. 9 (a), similar trends are observed along the detonation tube. An increase in the equivalence ratio increases pressure at the detonation wave front. The pressure at the detonation wave front is 17.30 atm, 18.22 atm, and 19.15 atm for ϕ=0.8, ϕ=1.0, and ϕ=1.2, respectively. C-J temperature for ϕ=0.8, ϕ=1.0, and ϕ=1.2 are 3640 K, 3673 K, and 3663 K, respectively [43]. As seen in Fig. 9(b), there are sudden increases in temperature values at the detonation wave front, similar to the pressure distribution. An increase in equivalence ratios is determined to increase the temperature at the detonation wave front. The ratios of the stable detonation wave front temperatures to the C-J

temperatures for ϕ=0.8, ϕ=1.0, and ϕ=1.2 are 0.840, 0.866, and 0.871, respectively.

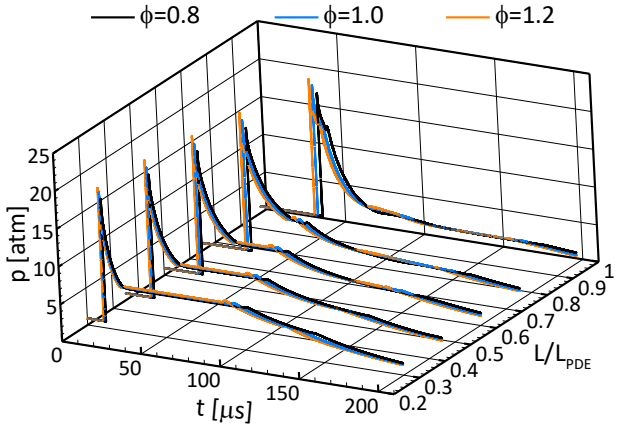

(a)

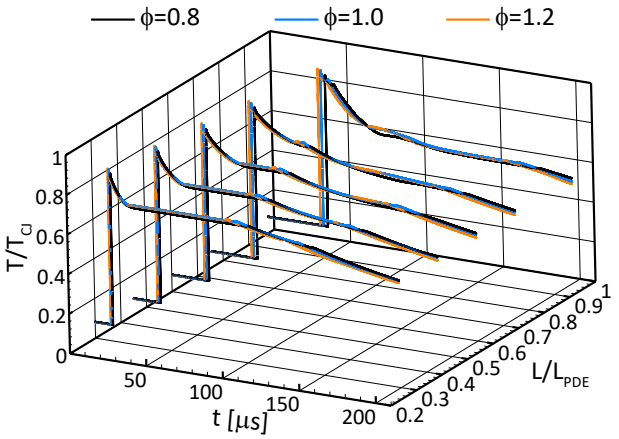

(b)

Fig. 9. a) Pressure and b) temperature ratio histories for different equivalence ratio

Detonation tube pressure profiles indicate that the DDT stage is completed quickly, similar to the validation case. When examining the flame position distribution given in Fig. 10, the linear development structure of the detonation wave velocity proves that the detonation wave is steady. An increase in equivalence ratio provided an increase in energy release, along with an increase in detonation wave velocity. The determined C-J velocity values for ϕ=0.8, ϕ=1.0, and ϕ=1.2 are 2654 m/s, 2836 m/s, and 2987 m/s, respectively [43]. The periods when the detonation wave separates from the detonation tube are, for ϕ=0.8, ϕ=1.0, and ϕ=1.2, respectively, 40.59 μs, 37.76 μs, and 35.66 μs. When examining the flame position distribution, the average detonation wave velocities ratios in the numerical studies to the C-J velocities for ϕ=0.8, ϕ=1.0, and ϕ=1.2 are 0.928, 0.933, and 0.938, respectively.

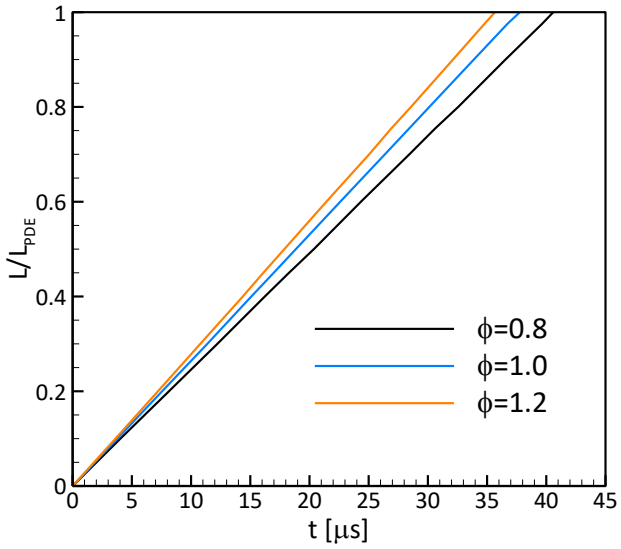

Fig. 10. Flame position for different equivalent ratio

During the blowdown stage, one of the pulse detonation engine cycle stages, the detonation wave transitions from the detonation tube to free space. No chemical reaction takes place during the blowdown stage. When examining the detonation wave propagation given in Fig. 11, it is observed that the detonation wave transforms from a planar to a spiral form.

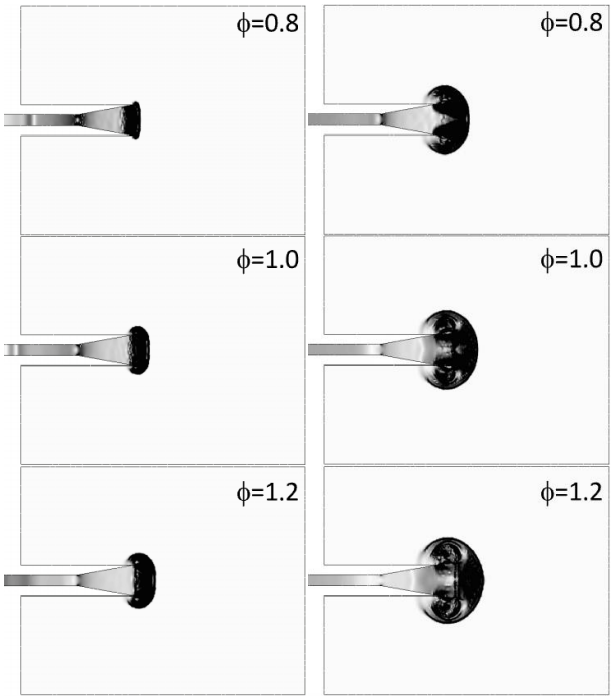

Fig. 11. Propagation of detonation wave in the nozzle and outlet domain at t= 60 μs (left side) and t= 70 μs (right side)

In Fig. 12, it can be observed that during the propagation of the detonation wave in free space, the reaction front and the leading shock front separate. After t=90 μs, discrete two wave fronts emerge, and it is understood that the propagation

velocity of the shock front is higher than that of the reaction front. A jet exhaust is formed at the center, and vortex sheets are observed behind the reaction front.

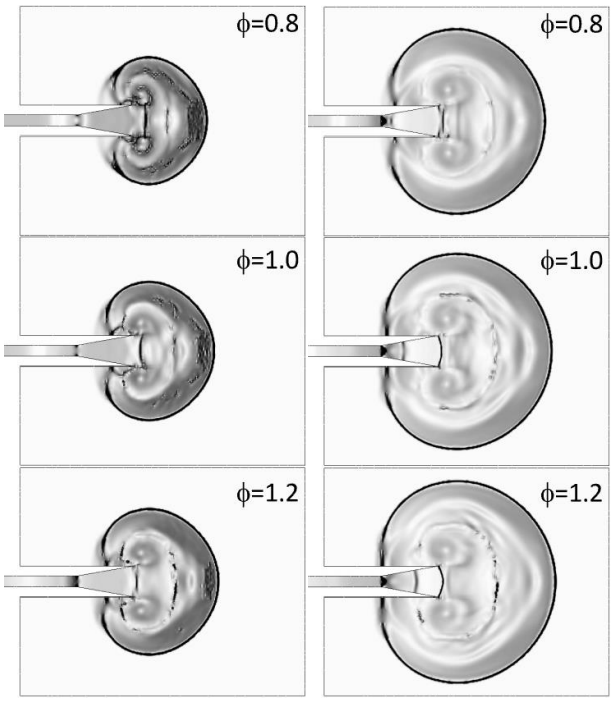

Fig. 12. Propagation of detonation wave in the nozzle and outlet domain at t= 90 μs (left side) and t= 110 μs (right side)

The detonation wave propagation within the nozzle and the blowdown stage directly affects the generated thrust. Fig. 13 provides the Mach number distribution at the nozzle exit. When examining the Mach number distribution at the nozzle exit, the time of the detonation wave's exit from the nozzle is 59.06 μs, 55.77 μs, and 53.53 μs for ϕ=0.8, ϕ=1.0, and ϕ=1.2, respectively. Sudden increases in the Mach number occur during the passage of the detonation wave through the nozzle exit. The rapid decrease in Mach number at the nozzle exit is due to the blowdown stage. The re-increase in the Mach number of the exhaust jet during the expansion of waves in the outlet domain serves as evidence. When examining the passage of the detonation wave from the nozzle exit, an increase in equivalence ratio results in an increased Mach number. The Mach numbers at the exit for ϕ=0.8, ϕ=1.0, and ϕ=1.2 are 1.302, 1.332, and 1.339, respectively. Similar trends are observed in the Mach number distribution at the nozzle exit after the blowdown stage.

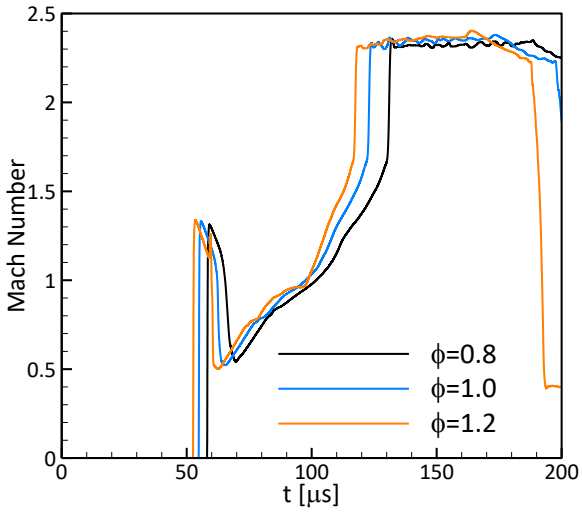

Fig. 13. Time evolution of the nozzle exit Mach Number for different equivalence ratio

To examine the changes in the nozzle performance with variations in the equivalence ratio of the fuel-oxidizer mixture, in Fig. 14 the evolution of pressure ratio at the nozzle exit is given. The pressure ratio distribution at the nozzle exit follows a similar trend to the Mach number at the nozzle exit. Sudden increases occur in the pressure ratio at the nozzle exit due to the high axial velocity. Decreases in total pressure due to the blowdown stage result in rapid drops in the pressure ratio. During the propagation of the detonation wave in the outlet domain and the pressure drop at the nozzle exit due to the jet exhaust, sudden increases in the pressure ratio are observed again. Increasing the equivalence ratio also increases the pressure ratio at the nozzle exit. The pressure ratios at the moment when the detonation wave separates from the nozzle are 2.783, 2.837, and 2.881 for ϕ=0.8, ϕ=1.0, and ϕ=1.2, respectively.

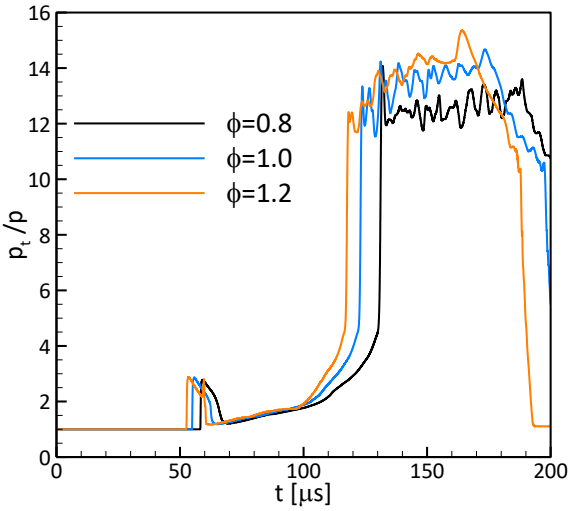

Fig. 14. Nozzle exit pressure ratio distribution for different equivalence ratio

To obtain the thrust distribution at the nozzle exit, the equation given in Equation (9) was used, where "*u*" is the axial velocity, and "$\boldsymbol{p}_{\infty}$" is the ambient pressure [44]. When examining the thrust distribution at the nozzle exit in Fig. 15, it is observed that there are sudden increases in the thrust distribution during the transition of the detonation wave. This is followed by another abrupt decrease due to the blowdown stage. The changes in the equivalence ratio result in similar trends in the thrust distributions at the nozzle exit. However, an increase in the equivalence ratio also increases the thrust values at the nozzle exit. This increase is higher from ϕ=1.0 to ϕ=1.2 compared to the increase from ϕ=0.8 to ϕ=1.0. After numerical studies, the thrust values generated at the moment of the detonation wave transition at the nozzle exit are 248.28 N, 264.5 N, and 270.83 N for ϕ=0.8, ϕ=1.0, and ϕ=1.2, respectively.

$$\boldsymbol{F}_{(t)} = \int_{exit} [\rho \boldsymbol{u}^2 + (\boldsymbol{p} - \boldsymbol{p}_{\infty})]\mathbf{d}\boldsymbol{A} \tag{9}$$

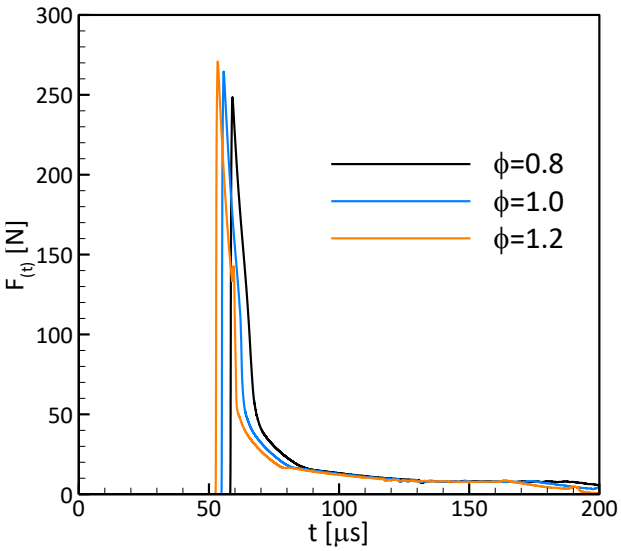

Fig. 15. Thrust distribution at the nozzle exit for different equivalence ratio

4. CONCLUSION

In this study, the effects of the fuel-oxidizer equivalence ratio on the propagation of the detonation wave and the performance of a pulse detonation engine are investigated numerically. In the numerical simulations, the pressure and temperature values of the fuel-oxidizer mixture were kept constant. Equivalence ratios of ϕ=1.2, ϕ=1.0, and ϕ=0.8 were chosen for rich, stoichiometric, and lean combustion conditions, respectively. The results obtained from the numerical simulations are listed below:

- The validation study was in good agreement with the reference experimental study. Following the DDT stage, the reference experimental study determined that the pressure at the detonation wave front is approximately 17 atm. In the numerical validation study, the pressure at the steady detonation wave front was determined to be 17.55 atm. While the average detonation wave velocity in the reference experimental study was 2737 m/s, it was found to be 2614 m/s in the numerical simulations.
- In the reference experimental study, it was understood that a stable detonation wave structure was obtained at the L/L_{PDE}=0.45 position. The numerical validation study observed that the DDT stage ended much more quickly, and a stable detonation wave was achieved
- The suitability of the AMR method for reducing the requirements of numerical simulations was investigated. The pressure gradient variable was used to split and recombine the cells. In the AMR method, the detonation wave front and the cells behind it were split into three stages, reducing the average minimum cell size to 0.1 mm. The average cell number ratio was 0.382 during the propagation of the detonation wave, and this method could significantly reduce the requirements for numerical simulations of detonation-based engines.
- During the blowdown phase, sudden decreases in Mach number and pressure ratio were identified at the nozzle exit. It was determined that a central jet exhaust and vortex sheets occurred during the propagation of the detonation wave in the outlet domain. At this stage, sudden increases in Mach number and pressure ratios were again observed at the nozzle exit.
- With the increase in equivalence ratio, temperature, and pressure values were observed at the detonation wave front. Additionally, it was observed that the detonation wave velocity increased with the rising equivalence ratio.
- At the nozzle exit, an increase in the equivalence ratio provided an increase in Mach Number, thrust, and pressure ratio values.

Conflicts of Interest

The author declares no conflict of interest.

REFERENCES

[1] L.-F. Zhang, S.-J. Zhang, Z. Ma, M.-Y. Luan, J.-P. Wang, Three-dimensional numerical study on rotating detonation engines using reactive Navier-Stokes equations. *Aerospace Science and Technology,* 93, 2019: 1–10. https://doi.org/10.1016/j.ast.2019.07.004

[2] E.M. Braun, F.K. Lu, D.R. Wilson, J A. Camberos, Airbreathing rotating detonation wave engine cycle analysis. *Aerospace Science and Technology*, 27(1), 2013: 201–208. https://doi.org/10.1016/j.ast.2012.08.010

[3] P. Wolański, Detonative propulsion. *Proceedings of the Combustion Institute*, 34(1), 2013: 125–158. https://doi.org/10.1016/j.proci.2012.10.005

[4] S. Prakash, V. Raman, C. Lietz, W.A. Hargus, S.A. Schumaker, High Fidelity Simulations of a Methane-Oxygen Rotating Detonation Rocket Engine. *AIAA Scitech 2020 Forum*, 6-10 January 2020, Orlando, Florida. https://doi.org/10.2514/6.2020-0689

[5] A.C. St. George, R. Driscoll, V. Anand, D.E. Munday, E.J. Gutmark, Fuel Blending as a Means to Achieve Initiation in a Rotating Detonation Engine. *53rd AIAA Aerospace Sciences Meeting*, 5-9 January 2015, Kissimmee, Florida. https://doi.org/10.2514/6.2015-0633

[6] B.R. Bigler, E.J. Paulson, W.A. Hargus, Idealized Efficiency Calculations for Rotating Detonation Engine Rocket Applications. *53rd AIAA/SAE/ASEE Joint Propulsion Conference*, 10-12 July 2017, Atlanta, USA. https://doi.org/10.2514/6.2017-5011

[7] J. Sousa, G. Paniagua, E. Collado Morata, Thermodynamic analysis of a gas turbine engine with a rotating detonation combustor. *Applied Energy*, 195, 2017: 247–256. https://doi.org/10.1016/j.apenergy.2017.03.045

[8] T. Suzuki, A. Matsuo, Y. Daimon, H. Kawashima, A. Kawasaki, K. Matsuoka, J. Kasahara, Prediction of Pressure Loss in Injector for Rotating Detonation Engines Using Single-element Simulations. *AIAA Propulsion and Energy 2020 Forum*, 24-28 August 2020. https://doi.org/10.2514/6.2020-3879

[9] R. Driscoll, W. Stoddard, A.S. George, E. Gutmark, Shock Transfer and Shock-Initiated Detonation in a Dual Pulse Detonation Engine/Crossover System. *AIAA Journal*, 53(1), 2015: 132–139. https://doi.org/10.2514/1.j053027

[10] T. Bussing, G. Pappas, An introduction to pulse detonation engines. *32nd Aerospace Sciences Meeting and Exhibit*, 10-13 January 1994, Reno, USA. https://doi.org/10.2514/6.1994-263

[11] K. Kailasanath, Review of Propulsion Applications of Detonation Waves. *AIAA Journal*, 38(9), 2020: 1698–1708. https://doi.org/10.2514/2.1156

[12] O. Kocaaslan, T. Yasa, K. M. Güleren, A parametric study on the swirler for turbulent combustion. *Journal of Thermal Science and Technology*, 41(2), 2021: 205-226. https://doi.org/10.47480/isibted.1025923

[13] M.N. Kaya, A.R. Kok, H. Kurt, Comparison of aerodynamic performances of various airfoils from different airfoil families using CFD. *Wind and Structures*, 32(3), 2021: 239-248. https://doi.org/10.12989/was.2021.32.3.239

[14] N. Alam, K.K. Sharma, K.M. Pandey, Numerical investigation of flame propagation and performance of obstructed pulse detonation engine with variation of hydrogen and air. *Journal of the Brazilian Society of Mechanical Sciences and Engineering*, 41(11), 2019: 502. https://doi.org/10.1007/s40430-019-2024-0

[15] N. Alam, K.K. Sharma, K.M. Pandey, Effects of Various Compositions of the Fuel-Air Mixture on the Pulse Detonation Engine Performance. *Combustion, Explosion, and Shock Waves*, 55(6), 2019: 708–717. https://doi.org/10.1134/s0010508219060121

[16] N. Alam, K.K. Sharma, K.M. Pandey, Numerical investigation of flame propagation in pulse detonation engine with variation of obstacle clearance. *Journal of Thermal Analysis and Calorimetry*, 140, 2019: 2485-2495. https://doi.org/10.1007/s10973-019-08948-5

[17] V.E. Tangirala, A.J. Dean, P.F. Pinard, B. Varatharajan, Investigations of cycle processes in a pulsed detonation engine operating on fuel–air mixtures. *Proceedings of the Combustion Institute*, 30(2), 2005: 2817–2824. https://doi.org/10.1016/j.proci.2004.08.208

[18] A.J. Dean, A. Rasheed, V. Tangirala, P.F. Pinard, Operation and Noise Transmission of an Axial Turbine Driven by a Pulse Detonation Combustor. *Turbo Expo 2005, Parts A and B , Vol.6,* 6-9 June 2005, Reno, USA. https://doi.org/10.1115/gt2005-69141

[19] D. Valiev, V. Bychkov, V. Akkerman, C.K. Law, L.-E. Eriksson, Flame acceleration in channels with obstacles in the deflagration-to-

detonation transition. *Combustion and Flame*, 157(5), 2010: 1012–1021. https://doi.org/10.1016/j.combustflame.2009.12.021

[20] A.V. Gaathaug, K. Vaagsaether, D. Bjerketvedt, Experimental and numerical investigation of DDT in hydrogen–Air behind a single obstacle. *International Journal of Hydrogen Energy*, 37(22), 2012: 17606–17615. https://doi.org/10.1016/j.ijhydene.2012.03.168

[21] I.O. Moen, M. Donato, R. Knystautas, J.H. Lee, Flame acceleration due to turbulence produced by obstacles. *Combustion and Flame*, 39(1), 1980: 21–32. https://doi.org/10.1016/0010-2180(80)90003-6

[22] T. Ogawa, V.N. Gamezo, E.S. Oran, Flame acceleration and transition to detonation in an array of square obstacles. *Journal of Loss Prevention in the Process Industries*, 26(2), 2013: 355–362. https://doi.org/10.1016/j.jlp.2011.12.009

[23] P. Debnath, K.M. Pandey, Computational Study of Deflagration to Detonation Transition in Pulse Detonation Engine Using Shchelkin Spiral. *Applied Mechanics and Materials*, 772, 2015: 136–140. https://doi.org/10.4028/www.scientific.net/amm.772.136

[24] S.M. Frolov, V.S. Aksenov, Deflagration-to-detonation transition in a kerosene-air mixture. *Doklady Physical Chemistry*, 416, 2007: 261–264. https://doi.org/10.1134/s0012501607090072

[25] K. Asato, T. Miyasaka, Y. Watanabe, K. Tanabashi, Combined effects of vortex flow and the Shchelkin spiral dimensions on characteristics of deflagration-to-detonation transition. *Shock Waves*, 23, 2013: 325–335. https://doi.org/10.1007/s00193-012-0430-7

[26] T. New, P. Panicker, F. Lu, H. Tsai, Experimental Investigations on DDT Enhancements by Schelkin Spirals in a PDE. *44th AIAA Aerospace Sciences Meeting and Exhibit*, 9-12 January 2006, Reno, USA. https://doi.org/10.2514/6.2006-552

[27] W. Wang, H. Qiu, W. Fan, C. Xiong, Experimental Study on DDT Characteristics in Spiral Configuration Pulse Detonation Engines. *International Journal of Turbo & Jet-Engines*, 30(3), 2013: 261-270. https://doi.org/10.1515/tjj-2013-0028

[28] F.K. Lu, E.M. Braun, Rotating Detonation Wave Propulsion: Experimental Challenges, Modeling, and Engine Concepts. *Journal of Propulsion and Power*, 30(5), 2014: 1125–1142. https://doi.org/10.2514/1.b34802

[29] J.T. Peace, F.K. Lu, Numerical Study of Pulse Detonation Engine Nozzle and Exhaust Flow Phenomena. *51st AIAA/SAE/ASEE Joint Propulsion Conference*, 27-29 July 2015, Orlando, Florida. https://doi.org/10.2514/6.2015-4189

[30] S.-J. Liu, Z. -Y. Lin, W. -D. Liu, W. Lin, M. -B. Sun, Experimental and three-dimensional numerical investigations on H_2/air continuous rotating detonation wave. *Proceedings of the Institution of Mechanical Engineers, Part G: Journal of Aerospace Engineering*, 227(2), 2012: 326–341. https://doi.org/10.1177/0954410011433542

[31] Z. Lei, X. Yang, J. Ding, P. Weng, X. Wang, Performance of rotating detonation engine with stratified injection. *Journal of Zhejiang University-SCIENCE A*, 21(9), 2020: 734–744. https://doi.org/10.1631/jzus.a1900383

[32] N. Tsuboi, Y. Watanabe, T. Kojima, A.K. Hayashi, Numerical estimation of the thrust performance on a rotating detonation engine for a hydrogen–oxygen mixture. *Proceedings of the Combustion Institute*, 35(2), 2015: 2005–2013. https://doi.org/10.1016/j.proci.2014.09.010

[33] J. Fujii, Y. Kumazawa, A. Matsuo, S. Nakagami, K. Matsuoka, J. Kasahara, Numerical investigation on detonation velocity in rotating detonation engine chamber. *Proceedings of the Combustion Institute*, 36(2), 2017: 2665–2672. https://doi.org/10.1016/j.proci.2016.06.155

[34] R. Zhou, J.-P Wang, Numerical investigation of shock wave reflections near the head ends of rotating detonation engines. *Shock Waves*, 23, 2013: 461–472. https://doi.org/10.1007/s00193-013-0440-0

[35] S. Yao, X. Han, Y. Liu, J. Wang, Numerical study of rotating detonation engine with an array of injection holes. *Shock Waves*, 27, 2016: 467–476. https://doi.org/10.1007/s00193-016-0692-6

[36] T.-H. Yi, J. Lou, C. Turangan, J.-Y. Choi, P. Wolanski, Propulsive Performance of a Continuously Rotating Detonation Engine. *Journal of Propulsion and Power*, 27(1), 2011: 171–181. https://doi.org/10.2514/1.46686

[37] S. Escobar, S. R. Pakalapati, I. Celik, D. Ferguson, P. Strakey, Numerical Investigation of Rotating Detonation Combustion in Annular Chambers. *Combustion, Fuels and Emissions,* Vol.1A, 3-7 June 2013, San Antonio, USA. https://doi.org/10.1115/gt2013-94918

[38] H. Zheng, Q. Meng, N. Zhao, Z. Li, F. Deng, Numerical investigation on H2/Air non-premixed rotating detonation engine under different equivalence ratios. *International Journal of Hydrogen Energy*, 45(3), 2020: 2289–2307. https://doi.org/10.1016/j.ijhydene.2019.11.014

[39] J. Sun, J. Zhou, S. Liu, Z. Lin, W. Lin, Effects of air injection throat width on a non-premixed rotating detonation engine. *Acta Astronautica*, 159, 2019: 189–198. https://doi.org/10.1016/j.actaastro.2019.03.067

[40] M.Ó Conaire, H.J. Curran, J.M. Simmie, W.J. Pitz, C.K. Westbrook, A comprehensive modeling study of hydrogen oxidation. *International Journal of Chemical Kinetics*, 36, 2004: 603–622. https://doi.org/10.1002/kin.20036

[41] C. Lietz, M. Ross, Y. Desai, W. A. Hargus, Numerical investigation of operational performance in a methane-oxygen rotating detonation rocket engine, *AIAA Scitech 2020 Forum*, 6-10 January 2020, Orlando, Florida. https://doi.org/10.2514/6.2020-0687

[42] T. Sato, V. Raman, Detonation Structure in Ethylene/Air-Based Non-Premixed Rotating Detonation Engine. *Journal of Propulsion and Power*, 36(15), 2020: 1-11. https://doi.org/10.2514/1.b37664

[43] NASA Glenn Research Centre, CEARUN rev4 (Chemical Equilibrium Applications) software, 2023. https://cearun.grc.nasa.gov/ (Accessed: 10 Jan 2024).

[44] T.-H. Yi, C. Turangan, J. Lou, P. Wolanski, J. Kindracki, A Three-Dimensional Numerical Study of Rotational Detonation in an Annular Chamber. *47th AIAA Aerospace Sciences Meeting Including the New Horizons Forum and Aerospace Exposition*, 5-8 January 2009, Orlando, Florida. https://doi.org/10.2514/6.2009-634